Lamacchia, E., Eckstein, E. N., Pirrera, A., & Weaver, P. M. (2015). Morphing structures: non-linear composite shells with irregular planforms. In 56th AIAA/ASCE/AHS/ASC Structures, Structural Dynamics, and Materials Conference. [0962] American Institute of Aeronautics and Astronautics Inc.. 10.2514/6.2015-0962

Morphing structures: non-linear composite shells with irregular planforms

E. Lamacchia*, E. Eckstein†, A. Pirrera‡and P.M. Weaver§

Advanced Composites Centre for Innovation and Science

University of Bristol, Queen's Building, University Walk, Bristol BS8 1TR, UK

The concept of morphing structures refers to devices that exhibit large scale shape changes, whilst maintaining load bearing capability, in response to distinctive operating conditions. This behavior comes from combinations of non-linear material or kinematic responses. Here, we limit our interests to shell type structures made from low strain, elastic materials that exhibit highly nonlinear kinematic behavior. Often, but not necessarily, the response can be bistable.

Models predicting the multistability of shells often present a compromise between computational efficiency and accuracy of results. Moreover, they deal mainly with regular domains, such as rectangular or elliptical planforms. Few studies have been done to investigate the performance and the possible advantages of exploiting multistable structures with more general domains.

In the present work, the multistability of thin shallow composite shells with irregular domains is investigated. An accurate and computationally efficient energy-based model is developed, in which the membrane and the bending components of the total strain energy are decoupled using the semi-inverse formulation of the constitutive equations. Transverse displacements are approximated using Legendre polynomials and the membrane problem is solved in isolation by combining compatibility conditions and equilibrium equations. The result is the total potential energy as a function of curvatures only. Stable shapes are recovered by minimizing the total energy with respect to curvature. The accurate evaluation of the membrane energy is a key step in order to accurately capture the bifurcation points. Here the membrane problem is solved using the Differential Quadrature Method (DQM), which provides accuracy at a relatively small computational cost. However, DQM is limited to rectangular domains. For this reason, blending functions are used to map the irregular physical domain into a regular computational domain.

This approach allows multistable shells with arbitrary convex planforms to be described without affecting the computational efficiency and the accuracy of the proposed model.

Nomenclature

u, v	In-plane displacements
w	Transverse displacements
$2L_x, 2L_y$	Dimensions of the shell along the Cartesian axes
Ω	Surface area
$\boldsymbol{n}$	Vector normal to the surface Ω
h	Shell thickness
$\boldsymbol{\varepsilon}$	Green-Lagrange strain tensor

*PhD Student, Advanced Composites Centre for Innovation and Science, University of Bristol, Queen's Building, University Walk, Bristol BS8 1TR, UK, Student Member AIAA.

†PhD Student, Advanced Composites Centre for Innovation and Science, University of Bristol, Queen's Building, University Walk, Bristol BS8 1TR, UK, Student Member AIAA.

‡Lecturer in Composite Structures, Advanced Composites Centre for Innovation and Science, University of Bristol, Queen's Building, University Walk, Bristol BS8 1TR, UK, Member AIAA.

§Professor in Lightweight Structures, Advanced Composites Centre for Innovation and Science, University of Bristol, Queen's Building, University Walk, Bristol BS8 1TR, UK, Member AIAA.

$\boldsymbol{\epsilon}$	Membrane strain tensor
$\boldsymbol{k}_0$	Curvature tensor of the undeformed configuration
$\boldsymbol{k}$	Curvature strain tensor of the deformed configuration
$\Delta\boldsymbol{k}$	Change in curvature from the undeformed to the deformed configuration
U_d, V_d, W_d	Coefficients used to scale the displacements
$\mathbf{E}$	Coefficients used to scale the in plane strains
$\mathbf{K}$	Coefficients used to scale the curvatures
$\boldsymbol{\sigma}$	Membrane stress tensor
$\boldsymbol{N}$	Membrane stress resultant
$\boldsymbol{\Sigma}$	Coefficients used to scale the membrane stress resultant
$\boldsymbol{M}$	Bending moment resultant
$\mathbf{Q}_k^*$	Lamina stiffness matrix
$\mathbf{A}$, $\mathbf{B}$, $\mathbf{D}$	In-plane, coupling and bending stiffness matrices respectively
Π	Total strain energy
Π_d	Coefficients used to scale the total strain energy
$\boldsymbol{\mathcal{L}}$	Differential operator
$\boldsymbol{\Sigma}_N$	Coefficients used to scale the thermoelastic stress resultant
$\boldsymbol{\Sigma}_M$	Coefficients used to scale the thermoelastic bending moment resultant
$\boldsymbol{\alpha}_k^*$	Secant thermal expansion coefficients of the lamina
T_0	Stress-free temperature
T_{ref}	Reference temperature
ΔT_0	Change in cure to room temperature
τ	Parameter used to characterise the thermal field
$P_l(\phi)$	Legendre polynomials
q_{ij}	Legendre parameters

Subscript

0	Undeformed reference surface
r	Inelastic deformation e.g. thermal, piezoelectric or moisture effects
k	Through the thickness position of the lamina

Superscript

$\sim$	Non-dimensional parameters

I. Introduction

Morphing shells are non-linear structures characterised by the ability to shape-change and often adopt multiple stable states. By exploiting this concept, designers may be able to devise structures able to adapt to a wide range of service conditions, resulting in more efficient structures that minimise both design complexity and cost.

A large variety of morphing concepts have been developed. These often utilise stiffness tailoring to provide shape changing features, such as non-symmetric composite plates[1] or prestressed laminates.[2] However, the main constraint traceable throughout all of them is the limiting variety of shapes that a single morphing device is actually able to achieve. It is perhaps intuitive that this limitation is mainly due to the geometric characteristics of the device itself, which narrow the range of possible configurations.

At present, non-linear models require high computational costs in order to accurately describe the multistability of shells. A further limitation is that most of the current works model regular domains, such as rectangular or elliptical planforms.

In this paper, we propose a robust and computationally efficient method to describe the multistability of thin shallow composite shells with irregular domains. As a consequence, we show the possibility of devising a novel class of morphing structure able to fulfill a wide range of applications compared with more conventional concepts.

Guest and Pellegrino[3] considered the stability of a cylindrical shell with constant curvature before Seffen[4]

generalised this approach to elliptic planforms with constant curvature whilst Vidoli[5] added quadratically varying curvature. Our approach builds upon these works by considering arbitrary-shaped planforms.

The total strain energy of a thin structure is expressed as the sum of the stretching and bending contributions. Once the problem is decoupled into these components, an auxiliary set of membrane problems is solved, combining the membrane equilibrium and constitutive equations. These equations link membrane strains and curvatures according to Gauss' Theorema Egregium.[6] The result is a membrane strain field which is a function of the curvatures. By substituting the strain field into the stretching energy, one obtains an expression for the total energy which is now a function of the curvatures only. Finally, the Hessian of the total energy with respect to the curvatures evaluates the stability of the resulting equilibrium shape.

The membrane strains can be solved in a closed form for an elliptic planform as done by Seffen.[4] Assuming constant curvature over the surface, Seffen uses the Airy stress function to solve the compatibility condition. Moreover, he expresses the membrane stress as a second order polynomial, which satisfies the boundary conditions of zero force and zero shear normal and tangent to the free boundary. Vidoli[5] relaxes the assumption of constant curvature over the surface, but he also observes that the limitation given by solving a series of auxiliary elliptic problems still holds, since the boundary conditions are satisfied exactly only for special geometries, i.e. shells with elliptic planforms or shells with lenticular cross section, as illustrated in Mansfield.[7]

The investigation of a membrane problem with arbitrary geometry calls for a numerical solution, as suggested in Vidoli and Maurini.[8] Following this observation, the present work solves the membrane problem by adopting an accurate and computationally efficient numerical method, i.e. the Differential Quadrature Method (DQM). Moreover, we are able to impose point-wise boundary conditions for the membrane problem, which are satisfied only in an average sense by in Vidoli.[5]

DQM was introduced by Bellman and Casti[9] and it is based on the premise that any continuous function can be approximated by a high-order polynomial in the overall domain, and that the derivative of a function can be expressed as a linear combination of the functional values at all the mesh points of the domain. Owing to the higher-order polynomial approximation, DQM usually requires fewer grid points in comparison to other approximation methods, such as Finite Element Method (FEM) or Finite Difference Method (FDM), to achieve accurate results.

The accuracy of the numerical method adopted to solve the membrane problem is crucial in order to evaluate the importance of each term in the energy functional. Other approximation methods, such as polynomial expansions for the in-plane displacement fields, leads to inefficiency in terms of computational costs, as shown by Mattioni et al.,[10] Aimmanee and Hyer[11] and Pirrera et al.[12] In this sense, DQM guarantees accuracy at a reduced computational cost.

However, DQM can be directly applied only to rectangular domains. For this reason, blending functions are used to map the irregular physical domain into a regular computational domain so that the DQM can be easily adapted to describe structures with arbitrary geometries. The feasibility of this approach has been already shown by Bert[13] and by Shu et al.[14] to analyse the vibration modes of irregular and curvilinear plates, respectively.

This paper is structured as follow: Section II illustrates the general model and its non-dimensional form. In Section III the model is validated against available benchmark results. Section IV describes the mapping technique using the blending functions. Here an interesting case study in which the morphing structure is not rectangular in planform is analysed. In particular, as a proof of concept we analyse the multistability of a thin-walled shell having a trapezoidal planform, similar to the chevron devices featured on modern civil airliners to reduce noise due to turbulent jet mixing.

II. Non-dimensional Model

A. Kinematics

In a Cartesian reference system x-y, the strains are defined in the usual form as a non-linear combination of linear deformations as:[15]

$$\boldsymbol{\varepsilon} = \boldsymbol{\epsilon} + z\boldsymbol{k}, \tag{1}$$

where

$$\begin{bmatrix}\epsilon_{xx}\\ \epsilon_{yy}\\ \epsilon_{xy}\end{bmatrix} = \begin{bmatrix}\dfrac{\partial u}{\partial x} + \frac{1}{2}\left(\dfrac{\partial w}{\partial x}\right)^2\\ \dfrac{\partial v}{\partial y} + \frac{1}{2}\left(\dfrac{\partial w}{\partial y}\right)^2\\ \left(\dfrac{\partial v}{\partial x} + \dfrac{\partial u}{\partial y} + \dfrac{\partial w}{\partial y}\dfrac{\partial w}{\partial x}\right)\end{bmatrix} \quad \text{and} \quad \begin{bmatrix}k_{xx}\\ k_{yy}\\ k_{xy}\end{bmatrix} = \begin{bmatrix}-\dfrac{\partial^2 w}{\partial x^2}\\ -\dfrac{\partial^2 w}{\partial y^2}\\ -2\dfrac{\partial^2 w}{\partial x \partial y}\end{bmatrix} \tag{2}$$

are the von-Kármán non linear mid-plane strains and curvature, respectively. Here u, v are the in-plane and w the transverse displacements.

In order to reduce possible numerical ill-conditioning of the non-linear model and to analyse the relative importance of each term in the governing equations, the following non-dimensional quantities are defined with the symbol *tilde* ($\tilde{}$):

$$\begin{array}{lll} x = L_x\tilde{x}, & y = L_y\tilde{y}, & \\ u = U_d\tilde{u}, & v = V_d\tilde{u}, & w = W_d\tilde{w}, \\ \boldsymbol{\epsilon} = \mathbf{E}\tilde{\boldsymbol{\epsilon}}, & \Delta\boldsymbol{k} = \mathbf{K}\Delta\tilde{\boldsymbol{k}}, & \boldsymbol{N} = \boldsymbol{\Sigma}\tilde{\boldsymbol{N}}. \end{array} \tag{3}$$

where $\Delta\boldsymbol{k} = \boldsymbol{k} - \boldsymbol{k}_0$ describes the change in curvature from the reference undeformed configuration to the current deformed configuration.

The dimensional parameters introduced in equation (3) are defined as:

- $2L_x$ and $2L_y$ are the dimensions of the plate along the cartesian axes.
- U_d, V_d and W_d are coefficients used to scale the displacements[12,16,17] defined as:

$$\begin{aligned} U_d &= \tfrac{1}{L_x}\sqrt[2]{\mathbf{A}^*_{11}\mathbf{A}^*_{22}\mathbf{D}^*_{11}\mathbf{D}^*_{22}}, \\ V_d &= \tfrac{1}{L_y}\sqrt[2]{\mathbf{A}^*_{11}\mathbf{A}^*_{22}\mathbf{D}^*_{11}\mathbf{D}^*_{22}}, \\ W_d &= \sqrt[4]{\mathbf{A}^*_{11}\mathbf{A}^*_{22}\mathbf{D}^*_{11}\mathbf{D}^*_{22}}, \end{aligned} \tag{4}$$

  where $\mathbf{A}^*$ and $\mathbf{D}^*$ are in-plane compliance and reduced bending stiffness terms, respectively.[18]

- $\mathbf{E}$ and $\mathbf{K}$ are scale the in plane strains and curvatures respectively and are defined as:

$$\mathbf{E} = \begin{bmatrix}\frac{1}{2}\dfrac{W_d^2}{L_x^2} & 0 & 0\\ 0 & \frac{1}{2}\dfrac{W_d^2}{L_y^2} & 0\\ 0 & 0 & \dfrac{W_d^2}{L_xL_y}\end{bmatrix}, \quad \mathbf{K} = \begin{bmatrix}-\dfrac{W_d}{L_x^2} & 0 & 0\\ 0 & -\dfrac{W_d}{L_y^2} & 0\\ 0 & 0 & -2\dfrac{W_d}{L_xL_y}\end{bmatrix}. \tag{5}$$

- $\boldsymbol{\Sigma}$ scales the membrane stress resultant $\boldsymbol{N}$ defined as $\boldsymbol{\Sigma} = \mathbf{AE}$.

B. Energy

The total potential energy is defined by using Claperyon's theorem as:[19]

$$\Pi = \int_\Omega \int_{-h/2}^{h/2} \frac{1}{2}\boldsymbol{\sigma}^\top \boldsymbol{\varepsilon}\, dz d\Omega, \tag{6}$$

where the stress tensor is:

$$\boldsymbol{\sigma} = \mathbf{Q}\left(\boldsymbol{\varepsilon} - \boldsymbol{\varepsilon}_r\right). \tag{7}$$

Here $\mathbf{Q}$ is the plate stiffness, Ω is the surface area, z represents the through the thickness coordinate and h is the plate thickness. The subscript r describes the contribution of any inelastic deformation e.g. thermal, piezoelectric or moisture effects; however for current purposes we will consider the thermal strains to be the sole contributors to inelastic deformations.

For a laminate plate, assuming $\mathbf{A}$, $\mathbf{B}$ and $\mathbf{D}$ to be the in-plane, coupling and bending stiffness matrices respectively, and defining $\boldsymbol{N}_r$ and $\boldsymbol{M}_r$ as the in-plane stress and moment resultants of the inelastic deformations, the total potential energy is written as:

$$\Pi = \int_{\Omega} \left(\frac{1}{2} \begin{bmatrix} \boldsymbol{\epsilon} \\ \Delta \boldsymbol{k} \end{bmatrix}^{\top} \begin{bmatrix} \mathbf{A} & \mathbf{B} \\ \mathbf{B} & \mathbf{D} \end{bmatrix} \begin{bmatrix} \boldsymbol{\epsilon} \\ \Delta \boldsymbol{k} \end{bmatrix} - \begin{bmatrix} \boldsymbol{N}_r \\ \boldsymbol{M}_r \end{bmatrix}^{\top} \begin{bmatrix} \boldsymbol{\epsilon} \\ \Delta \boldsymbol{k} \end{bmatrix} \right) d\Omega. \tag{8}$$

By substituting the semi-inverse constitutive relations expressed as:[18]

$$\begin{bmatrix} \boldsymbol{\epsilon} \\ \boldsymbol{M} + \boldsymbol{M}_r \end{bmatrix} = \begin{bmatrix} \mathbf{A}^* & \mathbf{B}^* \\ -\mathbf{B}^{*'} & \mathbf{D}^* \end{bmatrix} \begin{bmatrix} \boldsymbol{N} + \boldsymbol{N}_r \\ \Delta \boldsymbol{k} \end{bmatrix}, \tag{9}$$

into equation (8), where $\mathbf{A}^* = \mathbf{A}^{-1}$, $\mathbf{B}^* = -\mathbf{A}^{-1}\mathbf{B}$ and $\mathbf{D}^* = \mathbf{D} - \mathbf{B}\mathbf{A}^{-1}\mathbf{B}$, and where N and M are the vectors of the in-plane stress resultants and bending moments, the total potential energy in terms of non-dimensional parameters becomes:

$$\tilde{\Pi} = \int_{-1}^{1} \int_{-1}^{1} \left[\frac{1}{2} \tilde{\boldsymbol{N}}^{\top} \tilde{\mathbf{A}}^* \tilde{\boldsymbol{N}} + \frac{1}{2} \Delta \tilde{\boldsymbol{k}}^{\top} \tilde{\mathbf{D}}^* \Delta \tilde{\boldsymbol{k}} - \frac{1}{2} \tilde{\tau} \tilde{A}_r^* \tilde{\tau} - \tilde{\tau} \tilde{\mathbf{b}}_r^* \Delta \tilde{\boldsymbol{k}} - \tilde{\tau} \tilde{\mathbf{d}}_r^* \Delta \tilde{\boldsymbol{k}} \right] d\tilde{x} d\tilde{y}, \tag{10}$$

in the presence of an external thermal field characterised by τ. The non-dimensional matrices in the total strain energy are defined as:

$$\begin{aligned} \tilde{\mathbf{A}}^* &= \frac{L_x L_y}{\Pi_d} \boldsymbol{\Sigma}^{\top} \mathbf{A}^* \boldsymbol{\Sigma} = \frac{L_x L_y}{\Pi_d} \mathbf{E}\mathbf{A}\mathbf{E}, \\ \tilde{A}_r^* &= \frac{L_x L_y}{\Pi_d} \boldsymbol{\Sigma}_N^{\top} \mathbf{A}^* \boldsymbol{\Sigma}_N, \\ \tilde{\mathbf{b}}_r^* &= \frac{L_x L_y}{\Pi_d} \boldsymbol{\Sigma}_N^{\top} \mathbf{B}^* \mathbf{K}, \\ \tilde{\mathbf{D}}^* &= \frac{L_x L_y}{\Pi_d} \mathbf{K}^{\top} \mathbf{D}^* \mathbf{K}, \\ \tilde{\mathbf{d}}_r^* &= \frac{L_x L_y}{\Pi_d} \boldsymbol{\Sigma}_M^{\top} \mathbf{K}, \end{aligned} \tag{11}$$

where Π_d is used to scale the total potential energy and it is defined as:[12]

$$\Pi_d = \mathrm{tr} \left(\begin{bmatrix} \mathbf{E} & \mathbf{0} \\ \mathbf{0} & \mathbf{K} \end{bmatrix} \begin{bmatrix} \mathbf{A} & \mathbf{B} \\ \mathbf{B} & \mathbf{D} \end{bmatrix} \begin{bmatrix} \mathbf{E} & \mathbf{0} \\ \mathbf{0} & \mathbf{K} \end{bmatrix} \right). \tag{12}$$

In equation (11), the thermoelastic strains are $\boldsymbol{N}_r = \boldsymbol{\Sigma}_N \tilde{\tau}$ and $\boldsymbol{M}_r = \boldsymbol{\Sigma}_M \tilde{\tau}$, where $\tilde{\tau}$ is a non-dimensional parameter characterizing the temperature defined as:

$$\begin{aligned} T - T_{\mathrm{ref}} &= \Delta T_0 \tilde{\tau}, \\ \boldsymbol{\Sigma}_N &= \sum_{k=1}^{\mathrm{N_{ply}}} \int_{z_k}^{z_{k+1}} \mathbf{Q}_k^* (T) \, \boldsymbol{\alpha}_k^* (T) \, \Delta T_0 dz, \\ \boldsymbol{\Sigma}_M &= \sum_{k=1}^{\mathrm{N_{ply}}} \int_{z_k}^{z_{k+1}} \mathbf{Q}_k^* (T) \, \boldsymbol{\alpha}_k^* (T) \, \Delta T_0 z dz, \end{aligned} \tag{13}$$

in which ΔT_0 reflects the change in cure to room temperature and $\mathbf{Q}_k^* (T)$ and $\boldsymbol{\alpha}_k^* (T)$ are functions of temperature.

C. Compatibility Conditions

A generic Riemaniann manifold is completely characterised by its first and second fundamental form.[6] Components of the first and second fundamental forms are not independent and must satisfy the compatibility (or integrability) conditions. In two dimensions, these conditions reduce to three non-vanishing differential equations,[20] i.e. Gauss' Theorema Egregium and the Codazzi-Mainardi equations. They can be obtained from the Riemann tensor recast for a two-dimensional space. Physically, the compatibility relations between strains and curvatures represent the conditions of uniqueness of the normal vector at each point of the surface.

In particular, Gauss' Theorema Egregium plays a fundamental role in decoupling the membrane and bending contributions for our problem. It allows the compatibility condition, when combined with the equilibrium equations, to express the three components of the in-plane stress resultants as a function of curvatures only.

In the adopted Cartesian reference system and assuming small displacements and moderate rotations, the non-dimensional formulation of the compatibility condition for a thin shell is:

$$\frac{1}{2}\frac{\partial^2 \tilde{\epsilon}_{xx}}{\partial \tilde{y}^2} + \frac{1}{2}\frac{\partial^2 \tilde{\epsilon}_{yy}}{\partial \tilde{x}^2} - 2\frac{\partial^2 \tilde{\epsilon}_{xy}}{\partial \tilde{x}\partial \tilde{y}} = \tilde{k}_{xx}\tilde{k}_{yy} - 4\tilde{k}_{xy}^2 - \left(\tilde{k}_{0xx}\tilde{k}_{0yy} - 4\tilde{k}_{0xy}^2\right), \tag{14}$$

where the components of the non-dimensional membrane strains $\tilde{\boldsymbol{\epsilon}}$ and curvatures $\Delta\tilde{\boldsymbol{k}}$ are defined in equation (3).

Introducing the differential operator $\tilde{\mathcal{L}}_1$ defined as:

$$\tilde{\mathcal{L}}_1 = \frac{1}{2}\left[\frac{\partial^2}{\partial \tilde{y}^2}, \frac{\partial^2}{\partial \tilde{x}^2}, -4\frac{\partial^2}{\partial \tilde{x}\partial \tilde{y}}\right], \tag{15}$$

and the non-dimensional form of equation (9), the compatibility condition expressed in equation (14) can be recast as:

$$\tilde{\mathcal{L}}_1\left(\tilde{\boldsymbol{N}} - \tilde{\mathbf{B}}^*\tilde{\boldsymbol{k}} + \boldsymbol{\Sigma}^{-1}\boldsymbol{\Sigma}_N\tilde{\tau}\right) = \tilde{k}_{xx}\tilde{k}_{yy} - 4\tilde{k}_{xy}^2 - \left(\tilde{k}_{0xx}\tilde{k}_{0yy} - 4\tilde{k}_{0xy}^2\right). \tag{16}$$

D. Membrane Problem

The membrane problem is solved by combining equilibrium equations and compatibility conditions. For a free-free plate, the equilibrium of the in-plane stress resultants and the boundary conditions are:

$$\begin{cases} \dfrac{\partial N_x}{\partial x} + \dfrac{\partial N_{xy}}{\partial y} = 0, & \text{on } \Omega, \\ \dfrac{\partial N_{xy}}{\partial x} + \dfrac{\partial N_y}{\partial y} = 0, & \text{on } \Omega, \\ \boldsymbol{N}\cdot\boldsymbol{n} = 0, & \text{on } \partial\Omega, \end{cases} \tag{17}$$

where $\partial\Omega$ refers to the boundary of the plate Ω and $\boldsymbol{n}$ is its normal.

Introducing the differential operators $\boldsymbol{\mathcal{L}}_2$ and $\boldsymbol{\mathcal{L}}_3$ defined as:

$$\boldsymbol{\mathcal{L}}_2 = \begin{bmatrix} \dfrac{\partial}{\partial x} & 0 & 0 \\ 0 & 0 & \dfrac{\partial}{\partial x} \end{bmatrix}, \quad \boldsymbol{\mathcal{L}}_3 = \begin{bmatrix} 0 & 0 & \dfrac{\partial}{\partial y} \\ 0 & \dfrac{\partial}{\partial y} & 0 \end{bmatrix}, \tag{18}$$

the equilibrium equations assume the form:

$$\left(\boldsymbol{\mathcal{L}}_2 + \boldsymbol{\mathcal{L}}_3\right)\boldsymbol{N} = 0, \tag{19}$$

which is recast in terms of non-dimensional parameters as:

$$\frac{\sqrt{L_x L_y}}{\mathrm{tr}(\boldsymbol{\Sigma})}\left[\frac{1}{L_x}\tilde{\boldsymbol{\mathcal{L}}}_2\boldsymbol{\Sigma} + \frac{1}{L_y}\tilde{\boldsymbol{\mathcal{L}}}_3\boldsymbol{\Sigma}\right]\tilde{\boldsymbol{N}} = 0. \tag{20}$$

Finally, combining equation (16) and equation (20), the membrane problem is given by:

$$\begin{bmatrix} \tilde{\mathcal{L}}_1 \\ \frac{\sqrt{L_x L_y}}{\mathrm{tr}(\boldsymbol{\Sigma})}\left[\frac{1}{L_x}\tilde{\boldsymbol{\mathcal{L}}}_2+\frac{1}{L_y}\tilde{\boldsymbol{\mathcal{L}}}_3\right]\boldsymbol{\Sigma} \end{bmatrix}\tilde{\boldsymbol{N}} = \begin{bmatrix} \tilde{\mathcal{L}}_1\tilde{\mathbf{B}}^*\tilde{\boldsymbol{k}}+\tilde{k}_{xx}\tilde{k}_{yy}-4\tilde{k}_{xy}^2-\left(\tilde{k}_{0xx}\tilde{k}_{0yy}-4\tilde{k}_{0xy}^2\right) \\ 0 \end{bmatrix}, \tag{21}$$

where

$$\tilde{\mathbf{B}}^* = \boldsymbol{\Sigma}^{-1}\mathbf{B}\mathbf{K}. \tag{22}$$

Of great significance is that equation (21) gives the in-plane stress resultants $\tilde{\boldsymbol{N}}$ as functions of curvatures $\tilde{\boldsymbol{k}}$. Let us define

$$\tilde{\boldsymbol{\mathcal{L}}} = \begin{bmatrix} \tilde{\mathcal{L}}_1 \\ \frac{\sqrt{L_x L_y}}{\mathrm{tr}(\boldsymbol{\Sigma})}\left[\frac{1}{L_x}\tilde{\boldsymbol{\mathcal{L}}}_2+\frac{1}{L_y}\tilde{\boldsymbol{\mathcal{L}}}_3\right]\boldsymbol{\Sigma} \end{bmatrix}, \tag{23}$$

and

$$\boldsymbol{f} = \begin{bmatrix} \tilde{\mathcal{L}}_1\tilde{\mathbf{B}}^*\tilde{\boldsymbol{k}}+\tilde{k}_{xx}\tilde{k}_{yy}-4\tilde{k}_{xy}^2-\left(\tilde{k}_{0xx}\tilde{k}_{0yy}-4\tilde{k}_{0xy}^2\right) \\ 0 \end{bmatrix}. \tag{24}$$

The solution of the membrane problem is simply given by:

$$\tilde{\boldsymbol{N}} = \tilde{\boldsymbol{\mathcal{L}}}^{-1}\boldsymbol{f}, \tag{25}$$

which is a function of x, y and the curvature field $\Delta\tilde{\boldsymbol{k}}$.

In order to solve equation (25), it is necessary to discretise the matrix of differential operators defined in equation (23). This has been done using the matrix formulation of DQM. A comprehensive description of the DQM in matrix form can be found in Lamacchia et al.[21] By applying the DQM to equation (23), the differential operators $\tilde{\mathcal{L}}_1$, $\tilde{\boldsymbol{\mathcal{L}}}_2$ and $\tilde{\boldsymbol{\mathcal{L}}}_3$ are now matrices of weighting coefficients that we evaluate on a Chebyshev-Gauss-Lobatto mesh grid, which has been shown to be numerically efficient and well behaved.[22]

In order to find a general curvature field which satisfies equation (25), the out-of-plane displacements w have been approximated using the Legendre polynomials defined as:

$$w(x,y) = w_0(x,y) + \sum_{i=0}^{n}\sum_{j=0}^{n} q_{ij}P_i(x)P_j(y), \tag{26}$$

where w_0 is the reference (undeformed) shell configuration and q_{ij} are the Legendre parameters. Here $P_i(x)$ and $P_j(y)$ are the shape functions of order n given by the Legendre polynomials and they are defined using the binomial coefficient[23] as:

$$P_l(\phi) = \sum_{k=0}^{l}\binom{l}{k}\binom{-l-1}{k}\left(\frac{1-\phi}{2}\right)^k, \quad \text{for } l=i,j \text{ and } \phi=x,y. \tag{27}$$

Legendre polynomials are a complete set of orthogonal functions which have been shown to provide great robustness of results,[24] both in terms of accuracy and flexibility to describe the deformed shape of the laminate. For each value of n, w is a $2n$ order polynomial in x and y. Hence we approximate w with $(n+1)^2$ degrees of freedom, i.e. all the distinct combinations of the i and j indices of the q_{ij} parameters, from 0 to n.

Solving equation (25) involves the solution of a set of independent membrane problems whose number depends on the order n of the Legendre polynomial. In particular, for $n = 1, 2, 3, 4, ...$, one needs to solve $2, 17, 80, 233, ...$ independent membrane problems respectively. The DQM accurately captures this step of the proposed method with small computational cost, expecially given the relatively small number of mesh points necessary to achieve convergence of results compared to more conventional FEM or FDM.[22]

E. Equilibrium and Stability

The in-plane stress resultants $\tilde{\boldsymbol{N}}$ of equation (25) are functions of the Legendre parameters q_{ij}. By substituting $\tilde{\boldsymbol{N}}$ into equation (10) we have an expression of the total potential energy as a function of the q_{ij} only. The minima of the energy with respect to the q_{ij} give the equilibrium configuration:

$$\frac{\partial \tilde{\Pi}}{\partial q_{ij}} = 0. \tag{28}$$

The Hessian of the total potential energy with respect to the q_{ij} gives the stability position:

$$\frac{\partial^2 \tilde{\Pi}}{\partial q_{ij}^2} > 0. \tag{29}$$

Finally, the stable or unstable configurations that the laminate assumes are given by substituting the q_{ij} obtained from equation (28) back into equation (26).

III. Validation

A. Multi-mode Morphing

In Eckstein et al.[25] the deformations of an initially cylindrically curved unsymmetric $[0_4/90_4]$ laminate under thermal loads were studied. The combination of initial curvature and opposing thermal moments was found to give rise to multiple deformation modes. The laminate showed two orthogonal pure cylindrical shapes at curing and room temperature, and an intermediate twisting mode.

The authors formulated a Rayleigh-Ritz analytical model assuming a second order polynomial to approximate the out of plane displacements, with a resulting constant curvature tensor as in Dano et al.[26] The model was validated against a FEM simulation consisting of `256 ABAQUS S8R` elements, using a uniformly distributed converged mesh. The FEM and the Rayleigh-Ritz analytical model showed excellent agreement in predicting the two orthogonal cylindrical shapes. However, the analytical model overpredicted the values of curvatures in the range of temperatures when twisted configurations are present. The authors claimed that this limitation was due to the simple functions that were used to describe the in-plane strains, resulting in an overestimation of the membrane stiffness. This constraint makes it preferential for the laminate to store strain energy in the form of the bending component, hence the overprediction of the curvatures. The authors also observed that the approach adopted in Fernandes et al.[27] would likely yield more accurate results, because the membrane problem is first approximated with more degrees of freedom and then solved separately using an FEM. This model relies on the simplifying hypothesis of uniform curvature throughout the morphing process. Following the work done by Guest and Pellegrino,[3] Seffen[4] and Seffen et al.,[28] the global stability scenario can be described as function of curvature only.

As discussed in Section I, the present work follows a similar approach. Hence, the multi-mode morphing presented in Eckstein et al.[25] is used to validate our model and eventually show further insight.

Temperature-dependent material properties are taken into account, so that the non-dimensional matrices of the thermoelastic strains in equation (13) become:

$$\begin{aligned}
\boldsymbol{\Sigma}_N &= \sum_{k=1}^{N_{\text{ply}}} \int_{z_k}^{z_{k+1}} \mathbf{Q}_k^* (T) \left[\boldsymbol{\alpha}_k^* (T_0) (T_{\text{ref}} - T_0) / \tilde{\tau} + \boldsymbol{\alpha}_k^* (T) \Delta T_0 \right] dz, \\
\boldsymbol{\Sigma}_M &= \sum_{k=1}^{N_{\text{ply}}} \int_{z_k}^{z_{k+1}} \mathbf{Q}_k^* (T) \left[\boldsymbol{\alpha}_k^* (T_0) (T_{\text{ref}} - T_0) / \tilde{\tau} + \boldsymbol{\alpha}_k^* (T) \Delta T_0 \right] z dz, ,
\end{aligned} \tag{30}$$

in which T_0 is the stress-free temperature, $\boldsymbol{\alpha}_k^*$ are the secant thermal expansion coefficients as calculated from reference temperature T_{ref}. The terms in brackets express thermal strains for the case when $T_{\text{ref}} \neq T_0$, as is often the case in composite material data sets. In the case when $T_{\text{ref}} = T_0$ the terms in brackets collapse to their familiar form of equation (13).

B. Results and Discussion

Table 2 compares the curvatures given by the present model with the ones obtained analytically and numerically by Eckstein et al.[25] Material properties are obtained from reference [25] and reproduced in Table 1 for convenience. Results of the present model converge for a mesh grid of 31×31 nodes and for fourth order Legendre polynomials.

Table 2 shows that the current approach closely matches the cylindrical shapes obtained using the model presented in reference [25]. However, for values of temperature close to the twisted configurations some discrepancies arise. In particular, for $T = 90°\text{C}$, the analytical model in reference [25] overestimates the values of curvatures by predicting a twisted shape, whereas FEM and the present model predict the cylindrical configuration, with values of curvatures in excellent agreement.

Figure 1 shows the membrane and bending components of the total potential energy as a function of the temperature. As expected, by cooling down from the curing temperature (stress free configuration) to room temperature, the laminate reacts storing energy via membrane and bending components. It is interesting to observe how the membrane component increases as the laminate approaches the twisted configurations. As observed in reference [25], the maximum value of k_{xy} occurs at $T = 122°\text{C}$. This value of twist corresponds to the maximum value of membrane energy in Figure 1a. For the ranges of temperature where the cylindrical modes appear, the laminate behaves as a plate rather than a shell by storing strain energy in the form of bending rather than membrane component.

Table 1. Material properties as function of temperature.

T [°C]	CFRP						aluminium alloy 5251		
	E_{11}[GPa]	E_{22}[GPa]	G_{12}[GPa]	$\nu_{12}[-]$	$\alpha_{11}[10^{-6}/°\text{C}]$	$\alpha_{22}[10^{-6}/°\text{C}]$	E [GPa]	$\nu[-]$	α $[10^{-6}/°\text{C}]$
30	129.55	8.85	5.28	0.33	-2.3	23.4	72.0	0.33	23.00
60	127.99	8.42	4.88	0.33	-2.1	27.8	72.0	0.33	23.00
90	127.47	7.92	4.65	0.33	-1.5	28.6	70.6	0.33	23.10
120	127.18	7.57	4.50	0.33	-0.5	30.0	69.8	0.33	23.33
150	126.11	7.18	4.26	0.33	1.7	32.1	68.4	0.33	23.35
180	125.31	6.48	3.77	0.33	2.3	33.5	66.9	0.33	23.36

Table 2. Comparison of curvatures between the present model (order 4) and reference [25].

T [°C]	Analyitical ref. [25] $[m^{-1}]$			FEM ref. [25] $[m^{-1}]$			Present model $[m^{-1}]$		
	k_x	k_y	k_{xy}	k_x	k_y	k_{xy}	k_x	k_y	k_{xy}
30	-2.90	0	0	-2.90	0	0	-2.90	0	0
60	-2.30	0	0	-2.30	0	0	-2.30	0	0
90	-1.75	-0.10	-0.70	-1.75	0	0	-1.73	0	-0.01
120	-1.10	-0.90	-1.70	-1.09	-0.75	-1.60	-1.10	-0.79	-1.60
150	-0.30	-1.55	-1.45	-0.25	-1.55	-1.25	-0.25	-1.55	-1.30
180	0	-2.30	0	0	-2.3	0	0	-2.3	0

C. Conclusions

The validation of the proposed model against the work done by Eckstein et al.[25] showed how the correct evaluation of the membrane and bending components of the total strain energy influences the accuracy of the results. This accuracy has been achieved using the DQM to solve the membrane problem defined in equation (21). Moreover, by discretising the differential operator defined in equation (23), the membrane stress resultants have been evaluated by simply inverting a sparse matrix of weighting coefficients, as described in equation (25). This operation keeps the computational cost to acceptably low levels.

In the next section we show that the proposed model can be extended to shells of arbitrary convex planforms without affecting its accuracy. As a consequence, the aim is to provide an accurate and computationally efficient tool to devise a novel class of morphing structures able to fulfill a wide range of tasks compared to more conventional morphing concepts.

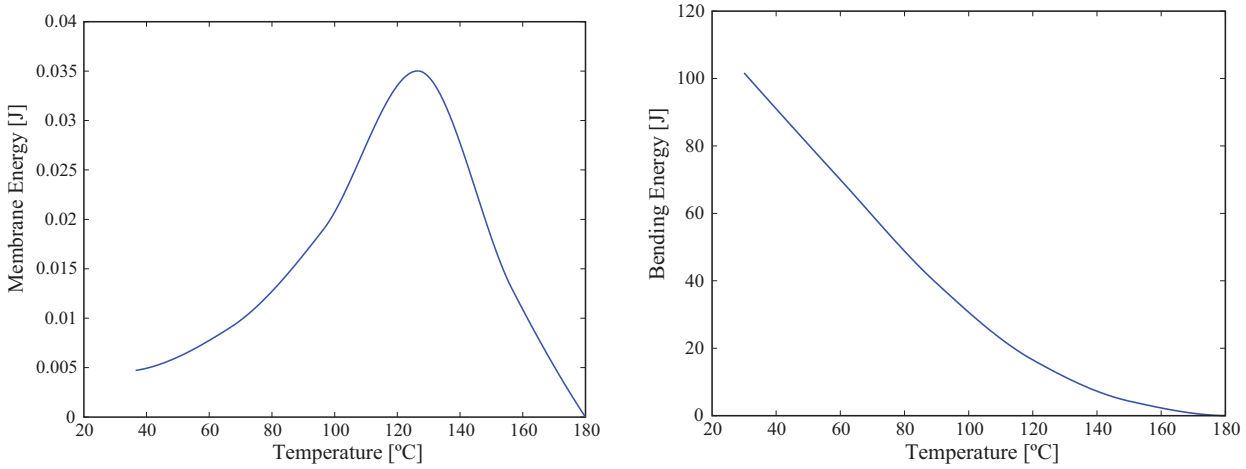

(a) Membrane energy.

(b) Bending energy

Figure 1. Membrane energy (a) and bending energy (b) as function of temperature.

IV. Multistability of Shells with Irregular Domain

In general, DQM provides accurate solutions with relatively low computational cost.[9,29] However, relatively little work has been done with irregular domains. Most of the applications of the DQM deal with regular domains having boundaries that are parallel to the coordinates axis.[30–32] Bert et al.[13] show the very first attempt to extend the DQM to irregular domains in the form of general curvilinear quadrilaterals using the mapping technique from the physical domain into a regular computational domain. In their work, the matrices of weighting coefficients in the computational domain are obtained applying the chain-rule. However, as observed by Shu et al.,[14] the dimension of the resulting matrices of weighting coefficients for the higher order derivatives is $(N_x N_y)^4$ compared to $(N_x N_y)^2$ for regular domains, where N_x and N_y are the number of grid points along x and y. This effect clearly influences the efficiency of the method. To overcome this limitation, Shu et al.[14] proposed that the governing and boundary conditions equations should be recast directly using the mapping technique, so that only the weighting coefficients for the first order derivatives are directly involved. Therefore, the conventional quadrature rule can be straightforwardly extended to capture irregular domains.

In this section, we show the flexibility of our model to describe irregular convex planforms, closely following the approach illustrated by Shu et al.[14] The equations derived in Section II are recast according to the transformation rules derived to map the irregular domain into the regular computational domain. In particular, the only expressions involved are the kinematics equations, the compatibility conditions and the boundary conditions. We observe that the computational cost, the accuracy in evaluating the membrane component of the total potential energy and hence the efficiency of the proposed model is not affected by the presence of irregular planforms.

A. Trapezoidal Domain

As a proof of concept, we analyse the multistability of a thin-walled shell having a trapezoidal planform, similar to the chevron devices featured on modern civil airliners. The aim is to provide a case study in which the candidate morphing structure is non-rectangular in planform. As depicted in Figure 2, a chevron is an aerodynamic device used on the trailing edge of aero-engine fan and exhaust nozzles to reduce noise due to turbulent jet mixing.[33] This noise reduction is accompanied by a drag penalty, and thus significant attention has been paid to developing Shape Memory Alloys (SMA)-actuated variable-geometry morphing chevrons, which can switch between low-noise and low-drag shapes.[34]

This case study aims to demonstrate that SMA-like behavior can also be achieved using conventional engineering materials acting in a Coefficient of Thermal Expansion (CTE)-mismatched bimorph arrangement. Ideally, the proposed chevron would be actuated by the temperature change between sea level and cruise altitude operation.

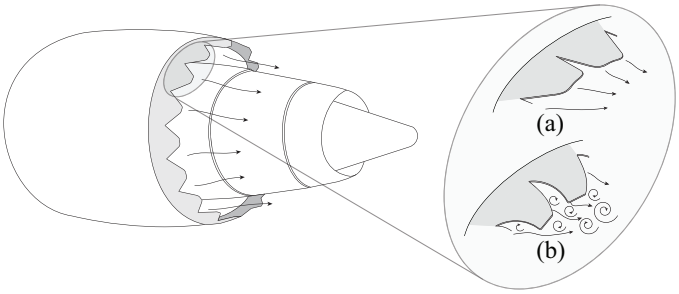

Figure 2. Illustration of a potential morphing chevron concept, whereby a number of vortex-generating devices are affixed to the trailing edge of a nozzle. These devices impinge upon the nozzle flow when deployed (b), encouraging mixing over shorter length scales and thus shifting jet noise to higher frequencies which are both less perceptible to the human ear and also attenuated faster when propagating through the atmosphere.[35] This action comes at a drag penalty, and thus it is desirable to stow the devices parallel to the local flow direction (a) at flight levels where community noise targets can be achieved without their aid.

We consider a hybrid aluminium/CFRP shell as proposed in Eckstein et al.[36] Material properties are a function of temperature and are listed in Table 1. With respect to the reference system of Figure 3, we consider an Al/ $[90_4]$ laminate, with CFRP having ply thickness of 0.26 mm and a 1.2 mm thick isotropic aluminium plate. The shell is clamped at the middle of the bottom edge. The temperature change is $\Delta T_0 = -150°\text{C}$, from the curing stress-free configuration at $T_0 = 180°\text{C}$ to room temperature $T_{\text{ref}} = 30°\text{C}$.

It is important to observe that, although the proposed morphing chevron seems an interesting solution for jet engine noise reduction, the aim of this work is not a detailed design of the chevron itself. Instead, we aim to provide a robust and computationally efficient method to devise novel class of morphing structures exploiting geometric feautures along with stiffness tailoring.

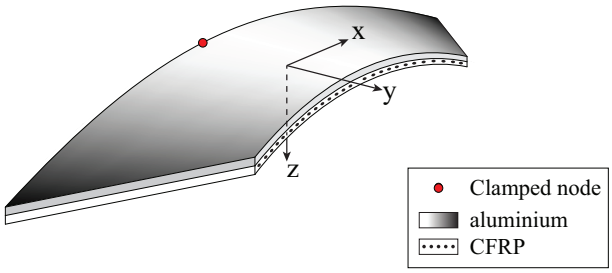

Figure 3. Hybrid laminate shell showing reference system and boundary conditions.

B. Blending Function

Let us consider the physical and computational domains of Figure 4. The points of the physical domain are identified by a set of x-y coordinates, Figure 4a. Each of these points is then mapped into the computational domain, identified by the ξ-η reference system of Figure 4b, through an appropriate system of transformation of coordinates defined by the vector $\boldsymbol{v}(\xi, \eta)$ as:

$$\boldsymbol{v}(\xi, \eta) = \begin{bmatrix} x(\xi, \eta) \\ y(\xi, \eta) \end{bmatrix}. \tag{31}$$

In order to find the rule to map the physical domain into the computational domain, let us consider the following linear blending function:[37]

$$\begin{aligned}\boldsymbol{v}(\xi,\eta) = &\left(\frac{1-\xi}{2}\right)P(-1,\eta) + \left(\frac{1+\xi}{2}\right)P(1,\eta) + \left(\frac{1-\eta}{2}\right)P(\xi,-1) + \left(\frac{1+\eta}{2}\right)P(\xi,1) \\ &- \frac{(1-\xi)(1-\eta)}{4}P(-1,-1) - \frac{(1-\xi)(1+\eta)}{4}P(-1,1) \\ &- \frac{(1+\xi)(1-\eta)}{4}P(1,-1) - \frac{(1+\xi)(1+\eta)}{4}P(1,1), \end{aligned} \quad (32)$$

where the functions $P(\xi_i,\eta)$ and $P(\xi,\eta_i)$ are the parametric curves that describe the original domain in terms of computational variables and where the the values $P(\pm1,\pm1)$ are the four corners of the computational domain corresponding to the analogous points in the physical domain.

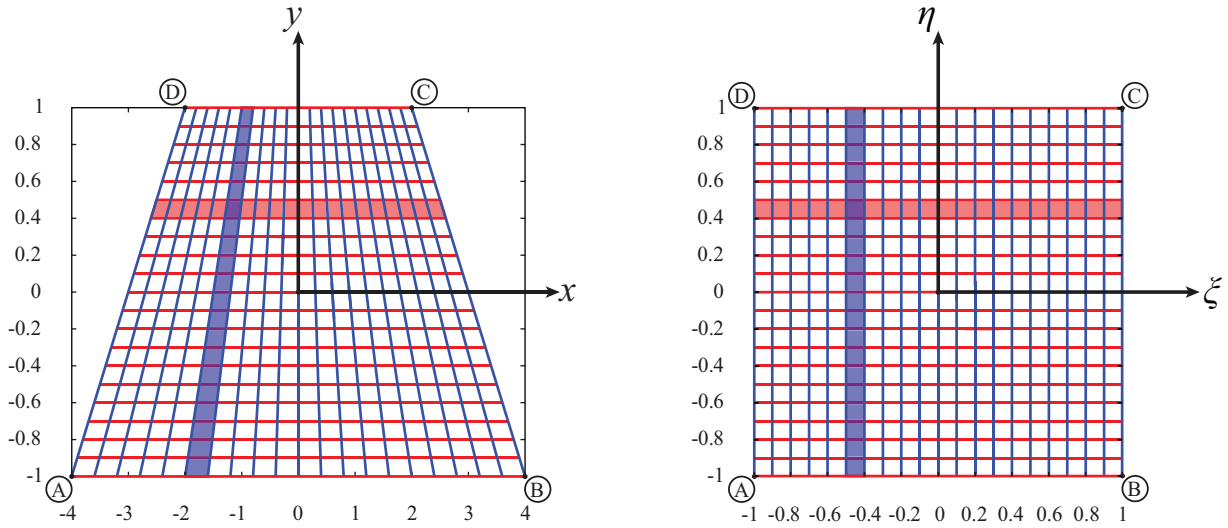

(a) Physical domain

(b) Computational domain

Figure 4. Physical domain (a) and computational domain (b) showing the relative reference systems.

For the non-rectangular domain of Figure 4a, the values of $P(\xi,\eta)$ in equation (32) are:

$$\begin{aligned} P(1,\eta) &= (-3+\eta,\eta), \\ P(-1,\eta) &= (3-\eta,\eta), \\ P(\xi,-1) &= (4\xi,-1), \\ P(\xi,1) &= (2\xi,1), \end{aligned} \quad (33)$$

and the four corners in the computational domain with respect to the coordinates of the physical domain are:

$$\begin{aligned} P(-1,-1) &= (-4,-1), \\ P(-1,1) &= (-2,1), \\ P(1,-1) &= (4,-1), \\ P(1,1) &= (2,1). \end{aligned} \quad (34)$$

Substituting equations (33) - (34) into equation (32), the mapping rule is given by:

$$\boldsymbol{v}(\xi,\eta) = \begin{bmatrix} x(\xi,\eta) \\ y(\xi,\eta) \end{bmatrix} = \begin{bmatrix} \xi(3-\eta) \\ (\eta) \end{bmatrix}. \quad (35)$$

In order to recast the governing equations in terms of the mapped domain, we need to express the partial derivatives in the computational domain using the *chain rule*. Given a general function $f(x,y)$, the partial

derivatives of f are:

$$\frac{\partial f}{\partial x_i} = \sum_i \frac{\partial f}{\partial \psi_i}\frac{\partial \psi_i}{\partial x_i}, \tag{36}$$

where $x_i = x, y$ and $\psi_i = \xi, \eta$. Applying equation (36) to equation (35), the partial derivatives of any function $g(\xi, \eta)$ in the computational domain corresponding to $f(x, y)$ in the physical domain are given by:

$$\begin{aligned} \frac{\partial f}{\partial x} &= \frac{1}{3-\eta}\frac{\partial g}{\partial \xi}, \\ \frac{\partial f}{\partial y} &= \frac{\xi}{3-\eta}\frac{\partial g}{\partial \xi} + \frac{\partial g}{\partial \eta}. \end{aligned} \tag{37}$$

Applying the expressions of the partial derivatives given in equation (37) to the membrane and out-of-plane displacements expressed in equation (2), the membrane strain and curvature tensors in the computational domain are:

$$\begin{bmatrix} \epsilon_{\xi\xi} \\ \epsilon_{\eta\eta} \\ \epsilon_{\xi\eta} \end{bmatrix} = \begin{bmatrix} \frac{1}{3-\eta}\frac{\partial u_0}{\partial \xi} + \frac{1}{2}\left(\frac{1}{3-\eta}\frac{\partial w_0}{\partial \xi}\right)^2 \\ \frac{\xi}{3-\eta}\frac{\partial v_0}{\partial \xi} + \frac{\partial v_0}{\partial \eta} + \frac{1}{2}\left(\frac{\xi}{3-\eta}\frac{\partial w_0}{\partial \xi} + \frac{\partial w_0}{\partial \eta}\right)^2 \\ \frac{\xi}{3-\eta}\frac{\partial u_0}{\partial \xi} + \frac{\partial u_0}{\partial \eta} + \frac{1}{3-\eta}\frac{\partial v_0}{\partial \xi} + \frac{1}{3-\eta}\frac{\partial w_0}{\partial \xi}\left(\frac{\xi}{3-\eta}\frac{\partial w_0}{\partial \xi} + \frac{\partial w_0}{\partial \eta}\right) \end{bmatrix}, \tag{38}$$

and

$$\begin{bmatrix} k_{\xi\xi} \\ k_{\eta\eta} \\ k_{\xi\eta} \end{bmatrix} = \begin{bmatrix} -\frac{1}{(3-\eta)^2}\frac{\partial^2 w_0}{\partial \xi^2} \\ -\frac{2\xi}{(3-\eta)^2}\frac{\partial w_0}{\partial \xi} - \frac{\xi^2}{(3-\eta)^2}\frac{\partial^2 w_0}{\partial \xi^2} - \frac{2\xi}{(3-\eta)}\frac{\partial w_0}{\partial \xi \partial \eta} - \frac{\partial^2 w_0}{\partial \eta^2} \\ -\frac{2}{(3-\eta)^2}\frac{\partial w_0}{\partial \xi} - \frac{2\xi}{(3-\eta)^2}\frac{\partial^2 w_0}{\partial \xi^2} - \frac{2}{(3-\eta)}\frac{\partial w_0}{\partial \xi \partial \eta} \end{bmatrix}. \tag{39}$$

Hence, the dimensional form of the differential operator defined in equation (15), and the differential operators defined equation (18), become:

$$\mathcal{L}_1 = \left[\xi^2\frac{\partial^2}{\partial \xi^2} + 2\xi\frac{\partial}{\partial \xi} + 2\xi(3-\eta)\frac{\partial^2}{\partial \xi \partial \eta} + (3-\eta)^2\frac{\partial^2}{\partial \eta^2}, \quad \frac{\partial^2}{\partial \xi^2}, \quad -2\frac{\partial}{\partial \xi} - 2\xi\frac{\partial^2}{\partial \xi^2} - 2(3-\eta)\frac{\partial^2}{\partial \xi \partial \eta} \right], \tag{40}$$

and

$$\boldsymbol{\mathcal{L}}_2 = \begin{bmatrix} \frac{1}{3-\eta}\frac{\partial}{\partial \xi} & 0 & 0 \\ 0 & 0 & \frac{1}{3-\eta}\frac{\partial}{\partial \xi} \end{bmatrix}, \quad \boldsymbol{\mathcal{L}}_3 = \begin{bmatrix} 0 & 0 & \frac{\xi}{3-\eta}\frac{\partial}{\partial \xi} + \frac{\partial}{\partial \eta} \\ 0 & \frac{\xi}{3-\eta}\frac{\partial}{\partial \xi} + \frac{\partial}{\partial \eta} & 0 \end{bmatrix}. \tag{41}$$

Two important observations at this point can be made:

- The Legendre polynomials used here that approximate the transverse displacements are now functions of ξ and η, because they have been obtained by applying the mapping rule given in equation (35) to equations (26) - (27) .
- The boundary conditions in equation (17) always refer to the physical domain. Hence, they need to be expressed in the physical planform accordingly before the mapping is done.

C. Results and Discussion

Results reported in Figure 5 show the stable configurations of the shell with trapezoidal planform as a function of temperature when a temperature change ΔT is applied. As was the case in the multi-mode morphing mechanism observed by Eckstein et al.[25] and reported in Section III, the hybrid shell deforms between two orthogonal cylindrical shapes at curing and room temperature through a series of intermediate twisted shapes for the range of temperatures around the bifurcation points. Our model shows that these

shape changes are the most energetically efficient to deform between two orthogonal cylindrical modes having curvatures of the same sign.

In the cylindrical configuration at $T = 30°\text{C}$, the flow is directed along the longitudinal axes of the engine and parallel to the ξ-η plane of the shell. At high temperature, the shell assumes a second cylindrical shape orthogonal to the initial one, so that it impinges the flux creating turbulence. This process is reversible, so by decreasing the temperature, the chevron deforms back into an orthogonal cylindrical configuration and the flux recovers a laminar condition. The morphing process is hence totally passive.

Results shown in Figure 5 converge at the fourth order Legendre polynomial $n = 4$, as shown in details in Table 3. It was observed that further increments of n led to negligible differences in w. Analogously, results reach convergence for a $N_\xi \times N_\eta = 31 \times 31$ Chebyshev-Gauss-Lobatto mesh grid.

Table 3. Convergence analysis for the transverse displacements w as function of the order n of the Legendre polynomials. The convergence analysis refers to the transverse displacements $w_{\mathbf{C}}$ and $w_{\mathbf{D}}$ of the two corners C and D reported in Figure 4.

T [°C]	n=2		n=3		n=4		n=5	
	w_{C}[cm]	w_{D}[cm]	w_{C}[cm]	w_{D}[cm]	w_{C}[cm]	w_{D}[cm]	w_{C}[cm]	w_{D}[cm]
180	1.501	1.501	1.505	1.505	1.506	1.506	1.506	1.506
150	1.162	1.162	1.165	1.165	1.169	1.169	1.169	1.169
120	0.0075	0.0078	0.0077	0.0079	0.0077	0.0089	0.0078	0.0089
90	0.0114	0.0115	0.0107	0.0128	0.0112	0.0133	0.0111	0.0133
60	0.4623	0.4623	0.4691	0.4691	0.4710	0.4710	0.4710	0.4710
30	0.4883	0.4883	0.4883	0.4883	0.4883	0.4883	0.4883	0.4883

V. Conclusions

By exploiting anisotropy of composite materials along with the inherent geometric nonlinearity of curved shells, these structures display unique and interesting behaviors, including multistability and temperature-triggered shape-morphing capability. In order to better predict these features, we have presented a robust and accurate energy-based semi-analytical model to describe the multistable behavior of laminate shells for morphing applications. The key step of the proposed method is the decoupling of the total strain energy into the stretching and bending contributions. We apply the DQM to solve the membrane problem, which allows the in-plane stress resultants to be found by simply inverting a sparse matrix of weighting coefficients. This process keeps the computational cost to acceptable low levels.

By using Legendre polynomials to approximate the transverse displacements, our model is able to accurately capture the values of the membrane and bending components of the total strain energy.

As an additional benefit, we have shown the flexibility of our model in describing the multistable behavior of thin laminate shells with arbitrary convex planforms. The accuracy and the efficiency of the proposed model are maintained when dealing with irregular domains, by mapping the physical irregular domain into a computational rectangular domain with blending functions. The governing equations have been recast according to a specific mapping law, so that the matrices of weighting coefficients used to solve the membrane problem are unchanged. As an example application, we have described the multistable behavior of a thermally-actuated hybrid aluminium/CFRP trapezoidal shell that resembles a morphing chevron for noise attenuation in jet engines. By using conventional engineering materials acting in a CTE-mismatched bimorph arrangement, the proposed multistable shell is actuated by the gradient of temperature through the exhaust gases flowing around the nozzle and outside the case. This makes the morphing structure totally passive, providing potential benefits compared to more conventional actuation systems.

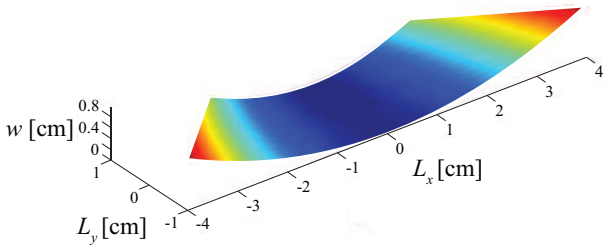

(a) $T = 30°\text{C}$, $\Delta T = -150°\text{C}$

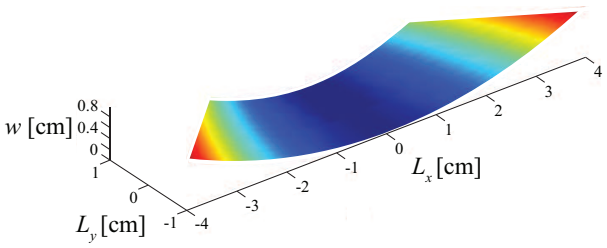

(b) $T = 60°\text{C}$, $\Delta T = -120°\text{C}$

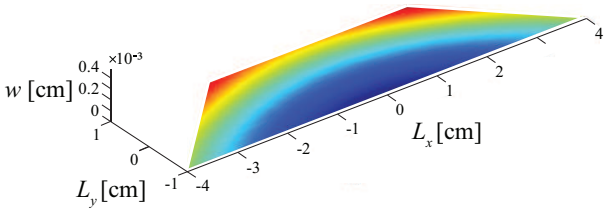

(c) $T = 90°\text{C}$, $\Delta T = -90°\text{C}$

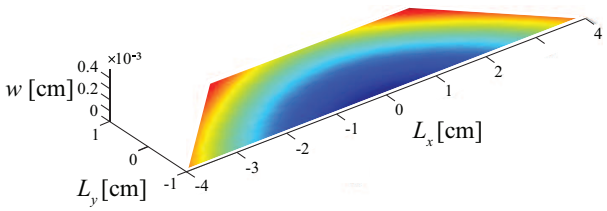

(d) $T = 120°\text{C}$, $\Delta T = -60°\text{C}$

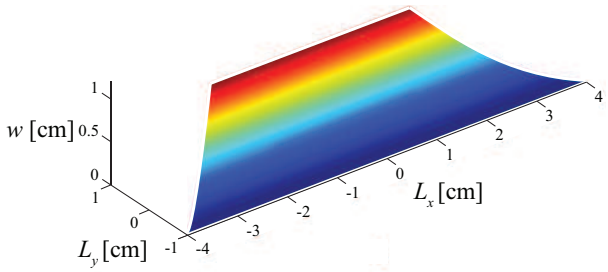

(e) $T = 150°\text{C}$, $\Delta T = -30°\text{C}$

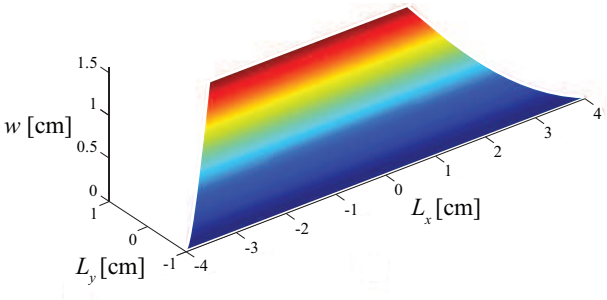

(f) $T = 180°\text{C}$, $\Delta T = 0°\text{C}$

Figure 5. Stable states of the multistable shell with trapezoidal planform as a function of the temperature when a temperature change ΔT is applied. The shell deforms between two orthogonal cylindrical configurations at curing and room temperature through a series of twisted modes for intermediate values of temperature. The color maps plotted onto the surfaces represent the transverse displacements w. Results are shown for Legendre polynomial of order $n = 4$ and $N_\xi \times N_\eta = 31 \times 31$ Chebyshev-Gauss-Lobatto mesh grid.

References

[1]Hyer, M. W., "Some Observations on the Cured Shape of Thin Unsymmetric Laminates," *Journal of Composite Materials*, Vol. 15, March 1981, pp. 175–194.

[2]Daynes, S., Potter, K. D., and Weaver, P. M., "Bistable prestressed buckled laminates," *Composites Science and Technology*, Vol. 68, No. 1516, 2008, pp. 3431 – 3437.

[3]Guest, S. D. and Pellegrino, S., "Analytical models for bistable cylindrical shells," *Proceedings of the Royal Society A: Mathematical, Physical and Engineering Science*, Vol. 462, 2006, pp. 839–854.

[4]Seffen, K. A., "Morphing bistable orthotropic elliptical shallow shells," *Proceedings of the Royal Society A: Mathematical, Physical and Engineering Science*, Vol. 463, 2007, pp. 67–83.

[5]Vidoli, S., "Discrete approximation of the Föppl-Von Kármán shell model: from coarse to more refined models," *International Journal of Solids and Structures*, Vol. 50, 2013, pp. 1241–1252.

[6]Novozhilov, V. V., "The theory of thin shells - A translation by Lowe P.G. and Radok J.R.M." *P. Noordhoff LTD*, Vol. 1, 1959, pp. 27–29.

[7]Mansfield, E. H., "Bending, buckling and curling of a heated thin plate." *Proceedings of the Royal Society A: Mathematical, Physical and Engineering Science*, Vol. 268, 1962, pp. 316–327.

[8]Vidoli, S. and Maurini, C., "Tristability of thin orthotropic shells with uniform initial curvature," *Proceedings of the Royal Society A: Mathematical, Physical and Engineering Science*, Vol. 464, 2008, pp. 2949–2966.

[9]Bellman, R. and Casti, J., "Differential quadrature and long-term integration," *Journal of Mathematical Analysis and Applications*, Vol. 34, No. 2, 1971, pp. 235–238.

[10]Mattioni, F., Weaver, P. M., and Friswell, M. I., "Multistable composite plates with piecewise variation of lay-up in the planform," *International Journal of Solids Structures*, Vol. 46 (1), 2009, pp. 151–164.

[11]Aimmanee, S. and Hyer, M. W., "Analysis of the manufactured shape of rectangular THUNDER-type actuators," *Smart Materials and Structures*, Vol. 13, No. 6, 2004, pp. 1389–1406.

[12]Pirrera, A., Avitabile, D., and Weaver, P. M., "Bistable plates for morphing structures: a refined analytical approach with high-order polynomials," *International Journal of Solids and Structures*, Vol. 47, No. 25-26, 2010, pp. 3412–3425.

[13]Bert, C. W. and Malik, M., "The differential quadrature method for irregular domains and application to plate vibration," *International Journal of Mechanical Sciences*, Vol. 38, No. 6, June 1996, pp. 589–606.

[14]Shu, C., Chen, W., and DU, H., "Free Vibration Analysis of Curvilinear Quadrilateral Plates by the Differential Quadrature Method," *Journal of Computational Physics*, , No. 163, pp. 452–466.

[15]Koiter, W. T., "On the Nonlinear Theory of Thin Elastic Shells." *Proc. Koninklijke Nederlandse Akademie van Wetenschappen*, Vol. 38, No. B69, 1966, pp. 1–54.

[16]Diaconu, C. G. and Weaver, P. M., "Postbuckling of long unsymmetrically laminated composite plates under axial compression," *International Journal of Solids and Structures*, Vol. 43, No. 2223, 2006, pp. 6978 – 6997.

[17]Nemeth, M. P., "Nondimensional parameters and equations for nonliner and bifurcation analyses of thin anisotropic quasi-shallow shells," *NASA/TP-2010-216726*, July 2010, pp. 589–606.

[18]Mansfield, E. H., "The bending and stretching of plates." *Cambridge University Press*, Vol. Second edition, 1989.

[19]Love, A. E. H., "A Treatise on the Mathematical Theory of Elasticity," *Cambridge*, Vol. 4th ed., 1927.

[20]McConnel, A. J., "Application of the Absolute Differential Calculus," *Blackie and Son Limited*, Vol. 1, 1931, pp. 193–207.

[21]Lamacchia, E., Pirrera, A., Chenchiah, I. V., and Weaver, P. M., "Non-axisymmetric bending of thin annular plates due to circumferentially distributed moments," *International Journal of Solids and Structures*, Vol. 51, No. 34, 2014, pp. 622 – 632.

[22]Shu, C., "Differential Quadrature and Its Application in Engineering," *Springer*, 2000.

[23]Koepf, W., "Hypergeometric Summation: An Algorithmic Approach to Summation and Special Function Identities," *Braunschweig, Germany: Vieweg*, 1998.

[24]Wu, Z., Raju, G., and Weaver, P., "Comparison of Variational, Differential Quadrature, and Approximate Closed-Form Solution Methods for Buckling of Highly Flexurally Anisotropic Laminates." *Journal of Engineering Mechanics*, Vol. 139, 2012, pp. 1073–1083.

[25]Eckstein, E., Pirrera, A., and Weaver, P. M., "Multi-mode morphing using initially curved composite plates," *Composite Structures*, Vol. 109, 2014, pp. 240–245.

[26]Dano, M.-L. and Hyer, M. W., "Thermally-induced deformation behavior of unsymmetric laminates," *International Journal of Solids and Structures*, Vol. 35, 1998, pp. 175–194.

[27]Fernandes, A., Maurini, C., and Vidoli, S., "Multiparameter actuation for shape control of bistable composite plates," *International Journal of Solids and Structures*, Vol. 47, 2010, pp. 1449–1458.

[28]Seffen, K. and McMahon, R., "Heating of a uniform wafer disk," *International Journal of Mechanical Science*, , No. 49, 2007, pp. 230–238.

[29]Bellman, R., Kashef, B., Lee, E., and Vasudevan, R., "Solving hard problems by easy methods: Differential and integral quadrature," *Computers and Mathematics with Applications*, Vol. 1, No. 1, 1975, pp. 133 – 143.

[30]Wangand, X., Bert, C. W., and G.Striz, A., "Buckling and vibration analysis of skew plates by the differential quadrature method," *AIAA J.*, Vol. 886, No. 32, 1994.

[31]Civan, F. and Sliepcevich, C. M., "Application of differential quadrature to solution of pool boiling in cavities," *Proc. Okla. Acad. Sci*, Vol. 73, No. 65, 1986.

[32]Striz, A. G., Chen, W., and Bert, C. W., "Static analysis of structures by the quadrature element method (QEM)," *International Journal of Solids and Structures*, Vol. 2807, No. 31, 1994.

[33]Bridges, J. and Brown, C. A., "Parametric Testing of Chevrons on Single Flow Hot Jets." *NASA/TM*, 213107- 2004.

[34]Mabe, J. H., Calkins, F. T., and Butler, G. W., "Boeing's Variable Geometry Chevron, Morphing Aerostructure for Jet Noise Reduction." *47th AIAA/ASME/ASCE/AHS/ASC Structures, Structural Dynamics, and Materials Conference*, 2142-2006.

[35]Bridges, J., Wernet, M., and Brown, C. A., "Control of Jet Noise Through Mixing Enhancement." *NASA/TM*, 212335-2003.

[36]Eckstein, E., Pirrera, A., and Weaver, P. M., "Thermally-Driven Morphing with Hybrid Laminates and Metal Matrix Composites," *Presented at AIAA SciTech Conference, Kissimmee, FL*, 5-9 January 2015.

[37]Gordon, W. J., "Blending-function methods of bivariate and multivariate interpolation and approximation," *Journal of Numerical Analysis*, Vol. 8, No. 151, 1971.